Non-LTE modelling of the HC2NC and HNC3 abundance in astrophysical environments

C. T. Bop, Benjamin Desrousseaux, F Lique

A&A 662, A102 (2022)
https://doi.org/10.1051/0004-6361/202243544

Astronomy & Astrophysics

Non-LTE modelling of the HC_2NC and HNC_3 abundance in astrophysical environments

C. T. Bop, B. Desrousseaux, and F. Lique

Univ. Rennes, CNRS, IPR (Institut de Physique de Rennes) – UMR 6251, 35000 Rennes, France
e-mail: cheikhtidiane.bop@ucad.edu.sn

Received 14 March 2022 / Accepted 27 April 2022

ABSTRACT

The isomers of HC_3N, namely HC_2NC and HNC_3, are widely observed in the interstellar medium and in circumstellar envelopes. Their abundance has been determined under the assumption of local thermodynamic equilibrium (LTE) conditions or non-LTE radiative transfer models, but in considering the collisional excitation of HC_3N as the same for all isomers. Chemical models for the prototypical cold cores, TMC-1 and L1544, reproduced the abundance of HC_3N fairly well, but they tend to overestimate the abundances of HC_2NC and HNC_3 with respect to the observations. It is therefore worth revisiting the interpretation of the observational spectra of these isomers using a rigorous non-LTE modelling. The abundance of HC_2NC and HNC_3 were then determined using non-LTE radiative transfer calculations based on the proper rate coefficients for the first time in this work. Modelling the brightness temperature of HC_2NC and HNC_3 when using their proper collision rate coefficients shows that models based on LTE or non-LTE with approximate collision data may lead to deviations of up to a factor of ∼1.5. Reinterpreting the observational spectra led us to significant differences relative to the observed abundances previously determined. Our findings suggest quite similar abundance ratios for the TMC-1 and L1544 cold cores as well as the L483 protostar. This work will encourage further modelling with more robust non-LTE radiative transfer calculations and future studies to revisit the chemistry of HC_3N and its isomers in cold molecular clouds.

Key words. scattering – molecular data – molecular processes – radiative transfer – ISM: abundances – ISM: molecules

1. Introduction

Understanding the formation and destruction paths of molecules is one of the most challenging issues in astrochemistry. Comparing the abundances of isomers observed in the interstellar medium (ISM) and circumstellar envelopes (CSEs) is a unique opportunity to gain better insights into the chemical processes yielding their formation and destruction. Interesting targets could be the isomers of HC_3N, namely HC_2NC and HNC_3, which are quite abundant in space.

Their detection towards TMC-1 (Kawaguchi et al. 1992b,a), IRC+10216 (Gensheimer 1997, 1998), L1544 (Jiménez-Serra et al. 2016; Vastel et al. 2018a), and L483 (Agúndez et al. 2019) encouraged extensive investigations on the chemistry underlying their synthesis. For instance, the chemical models of Osamura et al. (1999) and Vastel et al. (2018a) for the two prototypical cold cores TMC-1 and L1544, respectively, were constructed considering that HC_3N, HC_2NC, and HNC_3 mainly originate from the dissociative recombination of HC_3NH^+. Neutral-neutral reactions were also involved for the formation of HC_3N. With respect to the analysis of recent observational spectra by Cernicharo et al. (2020a) and Vastel et al. (2018a), these models reproduce the abundance of HC_3N fairly well, but they tend to overestimate the abundances of HC_2NC and HNC_3. For instance, the column density of HNC_3 derived from the chemical model for TMC-1 is greater than the value retrieved from the observational spectra by a factor of 5–10 (Vastel et al. 2018a). These disagreements may stem from poorly understood formation routes for the isomers of HC_3N and/or from the interpretation of the detected emission lines.

From the observational spectra, Vastel et al. (2018a) derived abundance ratios $N(HNC_3)/N(HC_3N)$ and $N(HC_2NC)/N(HC_3N)$ of $(0.31–1.25)\times10^{-2}$ and $(0.35–1.38)\times10^{-1}$, respectively, for the L1544 prestellar core. For the L483 protostar, Agúndez et al. (2019) reported $N(HNC_3)/N(HC_3N)\approx1.19\times10^{-3}$ and $N(HC_2NC)/N(HC_3N)\approx1.36\times10^{-2}$. For TMC-1 [IRC+10216], Cernicharo et al. (2020a) computed HNC_3 and HC_2NC abundances relative to HC_3N of $(2.26\pm0.3)\times10^{-3}$ and $(1.30\pm0.2)\times10^{-2}$ [$(0.75\pm0.08)\times10^{-3}$ and $(0.24\pm0.03)\times10^{-2}$], respectively.

Concerning chemical models, for TMC-1, Osamura et al. (1999) calculated abundances of $\sim4.2\times10^{-3}$ cm^{-3} and $\sim3.4\times10^{-2}$ cm^{-3} for HNC_3 and HC_2NC relative to HC_3N, respectively. For L1544, the chemistry[1] proposed by Vastel et al. (2018a) led to an abundance of $\sim\times10^{-1}$ for both HNC_3 and HC_2NC with respect to HC_3N. To the best of our knowledge, the chemistry of HC_3N and its isomers has not been studied for L483 and IRC+10216 yet.

In summary, the abundance ratios determined from observational spectra vary significantly from one source to another. The case of IRC+10216 must be treated separately since the chemistry in this region is different to that prevailing in cold cores (Cernicharo et al. 2020a). Among cold environments, the abundance ratios derived from the observations (chemical models) can differ by an order of magnitude (one to two orders of magnitude). Such drastic changes, for quite similar physical conditions and presumably the same chemistry, deserves to be reassessed.

[1] This chemical model is based on low-metal abundances and a H_2 volume density of 2×10^4 cm^{-3}.

When interpreting the observational spectra, the column densities of HC_2NC and HNC_3 were determined considering local thermodynamic equilibrium (LTE) conditions (Vastel et al. 2018a; Agúndez et al. 2019) or using radiative transfer calculations based on the rate coefficients of HC_3N (Cernicharo et al. 2020a). These two models are denoted hereafter as Model (1) and Model (2), respectively. Molecular abundances determined using Model (1) may not be accurate since the assumed LTE conditions are rarely reached in the ISM and CSE. For instance, Bop et al. (2021) show that LTE treatment could overestimate the abundance ratios $N(HNC_3)/N(HC_3N)$ and $N(HC_2NC)/N(HC_3N)$ by up to a factor of 2. On the other hand, the use of Model (2) to determine the abundance of isomers may be a source of bias since HC_3N, HC_2NC, and HNC_3 display different excitation schemes (Bop et al. 2019, 2021). It is, therefore, worth using each isomer's proper collisional data to model its abundance by means of radiative transfer calculations (this methodology is denoted hereafter as Model (3)) in order to draw more robust conclusions regarding the abundance ratios derived from the observations.

This paper aims to revisit the radiative transfer study of HC_2NC and HNC_3 in media where they were observed (TMC-1, IRC+10216, L483, and L1544) using the escape probability formalism along with the rate coefficients reported by Bop et al. (2021). It is important to note that previously only collisional rates of HC_3N were available in the literature (Wernli et al. 2007; Faure et al. 2016).

This paper is structured as follows: Sect. 2 presents a brief description of the scattering calculations and details of the radiative transfer study. In Sect. 3, we analyse and discuss the results and concluding remarks are given in Sect. 4.

2. Methods

The radiative transfer calculations were performed under the assumption of the escape probability formalism for a uniform expanding spherical shell as implemented in the `RADEX` computer code (Van der Tak et al. 2007). The molecular data (for HC_2NC and HNC_3) are composed of collision rate coefficients supplemented by the line frequencies, energy levels, and Einstein coefficients of the isomers. Apart from collision rate coefficients, the spectroscopic data were obtained from the Cologne Database for Molecular Spectroscopy (CDMS) portal (Endres et al. 2016).

The rate coefficients reported by Bop et al. (2021) were derived from integral inelastic cross sections induced by collision with ortho- and para-H_2 (hereafter denoted as o-H_2 and p-H_2, respectively). These data were calculated using the exact close-coupling quantum mechanical approach (Green 1975). These scattering calculations were based on potential energy surfaces (for HC_2NC–H_2 and HNC_3–H_2) computed at the CCSD(T)-F12b[2]/VTZ-F12[3] level of theory (Adler et al. 2007; Hill et al. 2010). More computational details can be found in Bop et al. (2019, 2021).

We calculated the brightness temperature (T_B), excitation temperature (T_{ex}), and the integrated intensity (W) for the $j_1 \rightarrow j_1 - 1$ ($j_1 = 1$–11) emission lines. Only the cosmic microwave background ($T_{CMB} = 2.73$ K) was included as a background radiation field. The full width at the half-maximum (FWHM) was set to 1 km s^{-1} since it does not affect the integrated intensity much. To fully cover the gas kinetic temperature (T) and the H_2 volume density [$n(H_2)$] of TMC-1, IRC+10216, L483, and L1544, that is to say the sources of interest, we smoothly varied T between 5 K and 50 K and $n(H_2)$ from 10^2 cm^{-3} to 10^8 cm^{-3}. For the H_2 volume density, we assumed different ortho-to-para ratios ($r_{o/p}$) following the thermal distribution. For example, $r_{o/p}$ was set to less than 1:100 for $T < 25$ K, ~1:10 for 25 K $\leq T \leq$ 40 K, and ~3:10 for $T > 40$ K. We note that these ratios do not affect the models much due to the moderate difference of the o- and p-H_2 rate coefficients. In case further modelling is needed, any ratio could be used since state-to-state rate coefficients for the HC_3N isomers due to collision with both o- and p-H_2 are available in the literature (Bop et al. 2021). The column density (N) of HC_2NC and HNC_3 was first set to 10^{10} cm^{-2} and then smoothly increased up to 10^{13} cm^{-2}. We also checked the opacity of the lines. The optical depth, which was calculated using a column density of 10^{12} cm^{-2} (10^{11} cm^{-2}), is found to be smaller than 0.06 (0.02) for HC_2NC (HNC_3). For more details, we refer the readers to Appendix A which presents the dependence of the opacities on the gas volume density.

3. Results

3.1. The excitation of HC_2NC and HNC_3

Bop et al. (2021) show that LTE conditions are reached for gas densities higher than 10^6 cm^{-3}, which is larger than the typical density in molecular clouds. For the excitation temperature, such an approximation may lead to errors of up to a factor of 2. Further discussions on the limits of the LTE approximation, in the case of HC_3N and its isomers, can be found in Bop et al. (2021).

To probe the relative increase or decrease in the brightness temperature upon the use of the proper rate coefficients of the isomers, we plotted the percentage change in T_B of Model (2) relative to that of Model (3) in Fig. 1. The analysis of these graphs is restricted to the region highlighted in grey ($10^3 \leq n$ (cm^{-3}) $\leq 10^5$) to simulate the typical gas density of astrophysical environments such as IRC+10216, TMC-1, L1544, and L483. For transitions involving low energy levels, Model (2) may underestimate the brightness temperature down to 10% in the case of HC_2NC and 15% in the case of HNC_3. On the other hand, when higher energy levels are involved, Model (2) leads to overestimation of up to 35% for HC_2NC and 40% for HNC_3. Regarding the temperature dependency, Model (2) does not correctly describe transitions among high-lying energy levels (e.g. 11 → 10) in the cold ($T = 10$ K) regime. For the warm ($T \geq 25$ K) regime, this model still fails at reproducing the brightness temperature for emission lines involving the lower rotational states (e.g. 1 → 0). The disagreement between Model (2) and Model (3) can be explained by the differences among the rate coefficients of HC_3N, HC_2NC, and HNC_3. Indeed, Bop et al. (2021) show that when using p-H_2 as a collider, the rate coefficients of HC_2NC and HNC_3 outweigh those of HC_3N by up to an order of magnitude. The large differences mostly concern the low temperature regime and transitions involving high-lying energy levels.

In summary, the accuracy of Model (2) depends on the transition, the temperature, and the isomer which points out its limits in modelling the following: (i) HNC_3 in any case; (ii) HC_2NC in the warm regime using low energy levels; and (iii) HC_2NC in the cold regime using high-lying energy levels. Since HC_2NC and HNC_3 were mainly observed through their $j_1 = 4$–11 → 3–10 emission lines (Kawaguchi et al. 1992b,a; Gensheimer 1998; Vastel et al. 2018a; Agúndez et al. 2019), accurate abundance

[2] Explicitly correlated coupled cluster with single, double, and non-iterative triple excitation.

[3] Polarized valence triple zeta Gaussian basis set which explicitly treats the correlation of electrons.

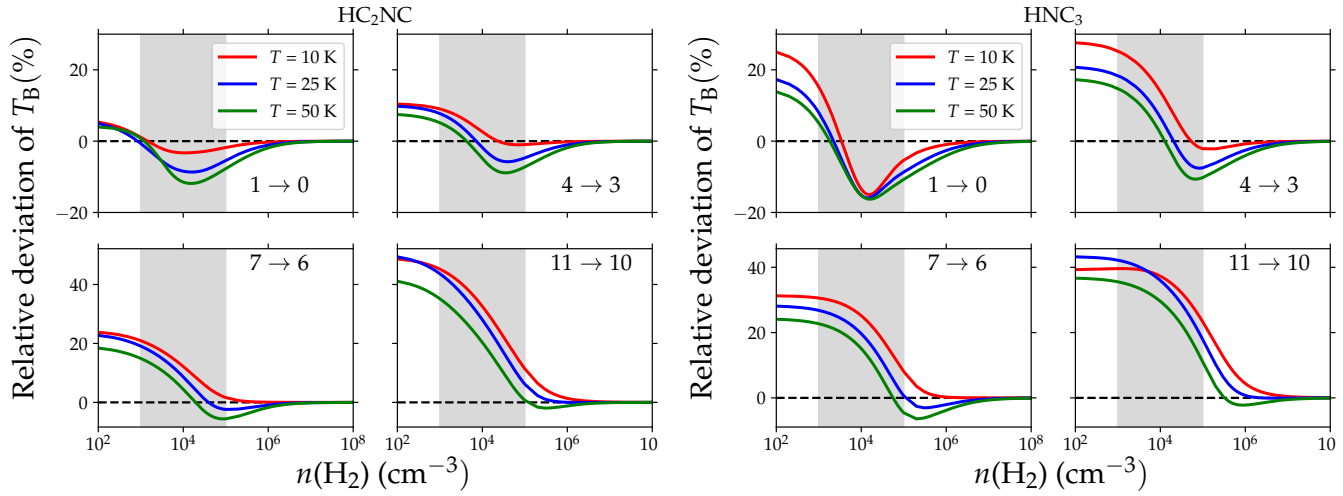

Fig. 1. Relative deviation of T_B upon Model (2) compared to Model (3) (see text for the description of the models) as a function of the H_2 volume density for selected temperatures and transitions. We note that HC_2NC and HNC_3 are represented in the *left* and *right* panels, respectively. These data were calculated for fixed column densities of 10^{12} cm^{-2}. The grey band delimits the region where $10^4 \leq n\,(\mathrm{cm}^{-3}) \leq 5\times10^4$.

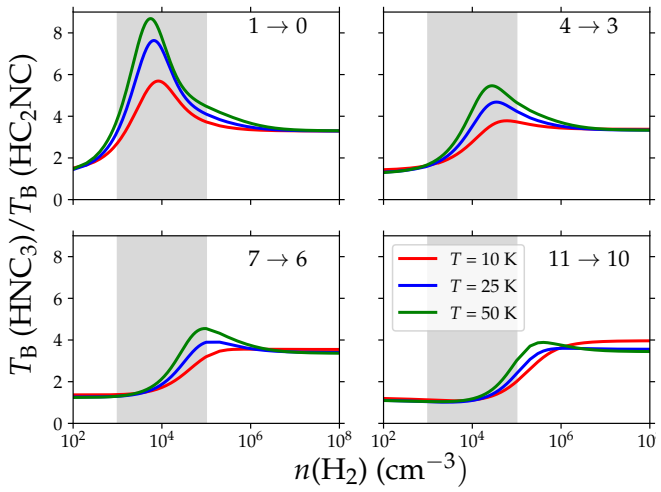

Fig. 2. Same as Fig. 1, but the *y* axis represents the HC_2NC and HNC_3 brightness temperature ratios calculated with Model (3).

modelling should be based on Model (3) or more robust radiative transfer calculations, but using the isomers' specific rate coefficients.

In Fig. 2, we plotted the brightness temperature ratio $[T_B(HNC_3)/T_B(HC_2NC)]$ as a function of the H_2 volume density for selected temperatures and transitions. Although more pronounced in transitions involving low energy levels, the brightness temperature ratio remains much greater than 1 for all emission lines. We note that there are some contributions due to the difference between the dipole moments of HC_2NC (2.93 D; Krüger et al. 1991) and HNC_3 (5.665 D; Botschwina et al. 1992). For example, the smallest ratio which occurs at 10 K for the $j_1 = 11 \rightarrow 10$ transitions can reach a value of 4 at $n(H_2) = 4\times10^5$ cm^{-3}. In the gas density range $[10^4 \leq n\,(\mathrm{cm}^{-3}) \leq 5\times10^4]$ relevant to astrophysical applications, the ratio varies between 2 and 6 for the most detected lines. Since the brightness temperature is proportional to the column density in the optically thin regime, equal line intensities would be obtained if the $N(HNC_3)/N(HC_2NC)$ abundance ratio was between 0.16 and 0.50.

3.2. Interpretation of the observational spectra of HC_2NC and HNC_3

To determine the abundances of HC_2NC and HNC_3, we assumed that the isomers are produced under the same physical conditions in all sources. In the modelling of Quénard et al. (2017) and Vastel et al. (2018a) for L1544 and that of Osamura et al. (1999) for TMC-1, the two species were assumed to form under the same physical conditions and mainly through the dissociative recombination of HC_3NH^+.

Since the frequencies of the observed lines differ by less than 20%, we expect that the inclusion of filling factors does not considerably change results (Vastel et al. 2014). Therefore, we also assumed that the sources fill the beams. We do not pretend to have interpreted the observational spectra using a sophisticated model, but to have made a sketch of the abundance ratio of the isomers in cold environments. Indeed, the non-LTE simulation of the HC_2NC and HNC_3 excitation using the `RADEX` radiative transfer code implied the use of a constant density and temperature. Such a treatment is well suited for TMC-1 and reasonably correct for L483 and IRC+10216, but much less adapted for L1544, because of its well-known density and temperature gradients (Quénard et al. 2017). Nevertheless, we expect the abundance ratio derived from our modelling to be relatively accurate.

Using the rate coefficients of HC_2NC and HNC_3 computed by Bop et al. (2021), we attempted to derive the column density of the isomers from the integrated intensities calculated in this work. The data, retrieved from the observational spectra of the isomers, to which we refer are presented in Table 1. In practice, the column density of the isomers and the H_2 volume density that best reproduce the observations were selected by calculating the χ^2 parameter (see Eq. (1)[4]):

$$\chi^2 = \sum_{i=1}^{n} \left(\frac{W_i^{\mathrm{obs}} - W_i^{\mathrm{cal}}}{\sigma_i} \right)^2 . \quad (1)$$

[4] W^{obs} and W^{cal} are the integrated intensities derived from the observations and our `RADEX` calculations, respectively. The index n stands for the number of observed lines and σ refers to the uncertainty on the measurements.

Table 1. Parameters of the HC_2NC and HNC_3 lines observed towards TMC-1, L1544, L483, and IRC+10216.

			Integrated intensities and linewidths							
	Frequency (MHz)		TMC-1 [a]		L1544 [b]		L483 [c]		IRC+10216 [d]	
Line	HC_2NC	HNC_3	HC_2NC	HNC_3	HC_2NC	HNC_3	HC_2NC	HNC_3	HC_2NC	HNC_3
4 → 3	39742.549	37346.541	164.7 ± 10 (0.62)	88.8 ± 10 (0.70)	–	–	–	–	75.0 ± 4 (–)	64 ± 7 (–)
5 → 4	49678.075	46683.061	138.4 ± 10 (0.58)	73.5 ± 10 (0.58)	–	–	–	–	78.0 ± 6 (–)	77 ± 7 (–)
8 → 7	79484.128	74692.105	–	–	73.4 ± 2.3 (0.41)	31.8 ± 5.6 (0.57)	–	–	–	–
9 → 8	89419.260	84028.240	–	–	44.0 ± 9.1 (0.37)	9.5 ± 4.0 (0.34)	39.0 ± 3.0 (0.43)	12.0 ± 1.0 (0.43)	–	–
10 → 9	99354.257	93364.241	–	–	29.2 ± 4.1 (0.44)	7.6 ± 2.0 (0.51)	26.0 ± 2.0 (0.46)	8.0 ± 1.0 (0.56)	–	–
11 → 10	109289.104	–	–	–	11.7 ± 3.5 (0.45)	–	15.0 ± 2.0 (0.44)	–	–	–

Notes. From column 4 to 11, the integrated intensities (in mK km s^{-1}) are given in the first entries and the linewidths (in km s^{-1}) are shown in the second entries. [a] Refers to Cernicharo et al. (2020a). [b] Refers to Vastel et al. (2018a). [c] Refers to Agúndez et al. (2019). [d] Refers to Cernicharo et al. (2020a).

The gas kinetic temperature of the regions of interest, TMC-1, L1544, L483, and IRC+10216, is well constrained in the literature. Therefore, we varied the temperature by 20% around (i) 10 K for TMC-1 (Cernicharo et al. 2020b) and L483 (Agúndez et al. 2019); (ii) 12 K for L1544 (Vastel et al. 2018b); and (*iii*) 37 K for IRC+10216. The latter was derived using the mass loss rate of Guélin et al. (2018) at 14″ from the star, which corresponds to the peak intensity of HC_3N (Agúndez et al. 2017). We note that a slight change in temperature does not substantially affect the χ^2 parameter.

In Fig. 3, we plotted the variation of the χ^2 parameter (for a single value of temperature) as a function of the H_2 volume density and the column density of the isomers for IRC+10216, TMC-1, L1544, and L483. For all sources, a large set of parameters (density of H_2 and column density of the isomers) allowed us to reproduce the observations with confidences better than 90%. We note that the lowest χ^2 value (marked with the white "+" sign in Fig. 3) may lead to unrealistic physical conditions. For example, in the case of L1544, the HC_2NC and HNC_3 column densities were obtained for $n(H_2) = 2.0 \times 10^4$ cm^{-3} and $n(H_2) = 2.5 \times 10^3$ cm^{-3}, respectively. Being out of the grey region, which is the typical H_2 density for cold molecular clouds and circumstellar envelopes, these solutions are not considered.

In summary, the solutions we are looking for must be located in the grey band and they must also correspond to similar H_2 density for both isomers. The column densities derived for all sources of interest, except IRC+10216, are summarized in Table 2 for comparison with the results available in the literature.

TMC-1. We obtained column densities of (1.0–1.7) $\times 10^{12}$ cm^{-2} and (1.8–2.7) $\times 10^{11}$ cm^{-2} for HC_2NC and HNC_3, respectively, at $n(H_2) = (1.0–4.0) \times 10^4$ cm^{-3}. From the analysis of the HC_3N emission lines, Cordiner et al. (2013) and Pratap et al. (1997) reported $n(H_2) \approx 1 \times 10^4$ cm^{-3} and $n(H_2) \approx 8 \times 10^4$ cm^{-3}, respectively, when using the same method. Concerning the column densities, we underestimated the column densities reported by Cernicharo et al. (2020a) by more than 50%.

Table 2. Column densities and abundance ratios of HC_2NC and HNC_3 derived for TMC-1, L1544, and L483.

	TMC-1	L1544	L483
HC_2NC (10^{12} cm^{-2})	1.0–1.7 3.0 ± 0.3 [a]	0.7–1.2 0.85–2.2 [b]	0.5–1.8 0.57 ± 0.28 [c]
HNC_3 (10^{11} cm^{-2})	1.8–2.7 5.2 ± 0.3 [a]	1.0–3.0 0.75–2.0 [b]	0.8–3.5 0.50 ± 0.25 [c]
$N(HC_2NC)/N(HNC_3)$	5.5–6.3 5.5 [a] ~8 [d]	4.3–7.0 4.3–29.3 [b] ~1 [e]	5.1–6.3 11.4 [c] –

Notes. For each line, the first and second entries (and third for the ratios) represent our results and those quoted from the literature, respectively. [a] Derived from the observations of Cernicharo et al. (2020a). [b] Derived from the observations of Vastel et al. (2018a). [c] Derived from the observations of Agúndez et al. (2019). [d] Derived from the chemical model of Osamura et al. (1999). [e] Derived from the chemical model of Vastel et al. (2018a).

L1544. For HC_2NC and HNC_3, we found column densities of (0.7–1.2) $\times 10^{12}$ cm^{-2} and (1.0–3.0) $\times 10^{11}$ cm^{-2}, respectively, at $n(H_2) = (1.5–4.0) \times 10^4$ cm^{-3}. We would like to point out that this gas density for L1544 is in agreement with the result (~10^4 cm^{-3}) of Vastel et al. (2018a) obtained from the modelling of HC_3N and HNC_3. The HC_2NC (HNC_3) column densities we computed are lower (higher) by 30–45% (35–50%) than the results of Vastel et al. (2018a).

L483. The observations were reproduced for $n(H_2) = (1.2–5.0) \times 10^4$ cm^{-3}. The gas density is in agreement with the value (~3×10^4 cm^{-3}) commonly used in the literature

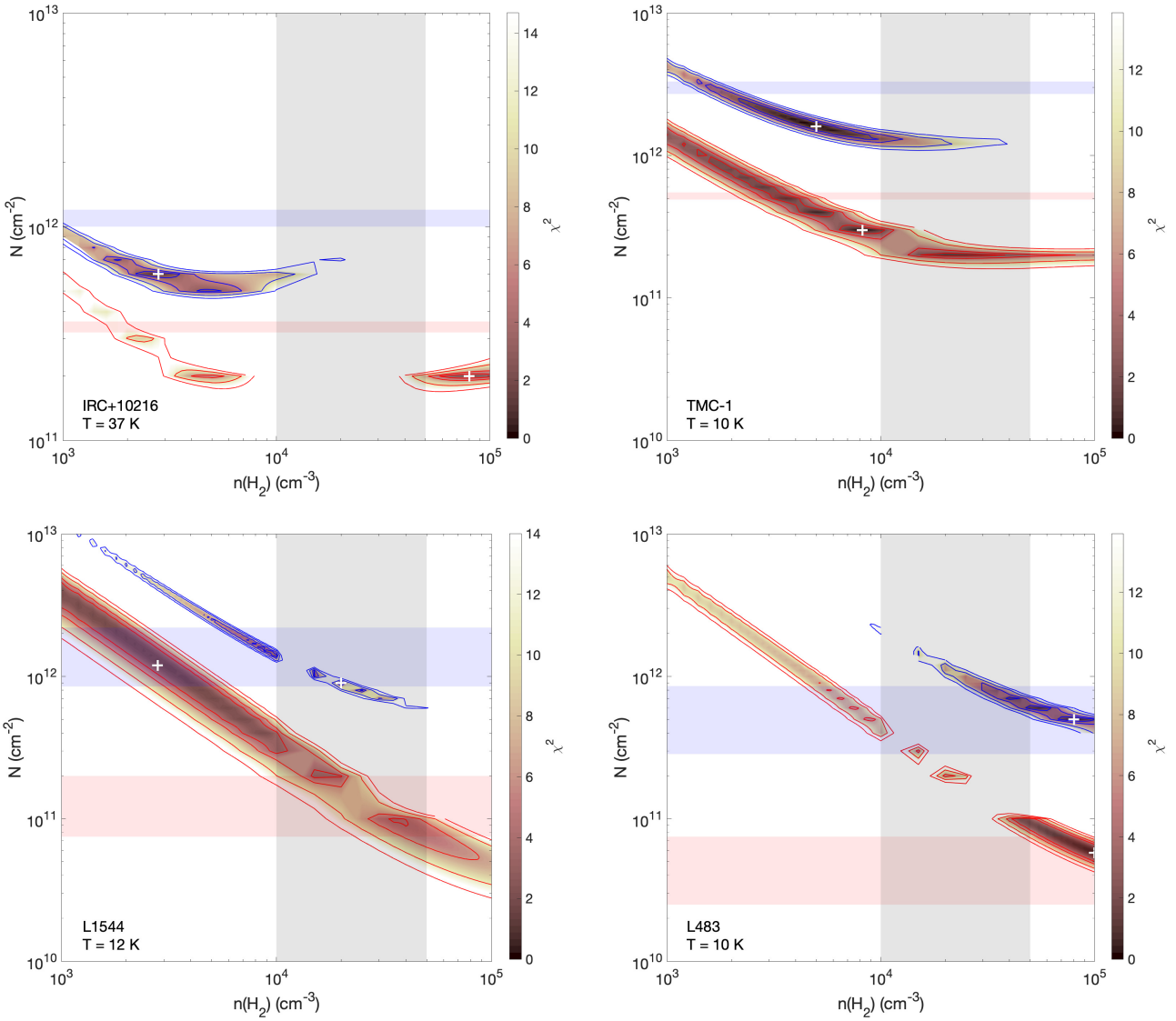

Fig. 3. Variation of the χ^2 parameter as a function of the H_2 volume density and the column densities of HC_2NC and HNC_3 for the sources of interest. The solid blue [red] lines represent confidence contour levels of 63.3%, 90.0%, 99.0%, and 99.9% (from the inner to outer contours) for the HC_2NC [HNC_3] isomer. The '+' symbol highlights the position of the minimum value of χ^2. The blue (red) and grey-shaded regions show the column density of HC_2NC (HNC_3) derived using Model (1) or Model (2) (see text) and the typical H_2 density in molecular clouds, respectively.

(Agúndez et al. 2019). For the column densities, we obtained $N(HC_2NC) = (0.5–1.8) \times 10^{12}$ cm^{-2} and $N(HNC_3) = (0.8–3.5) \times 10^{11}$ cm^{-2}, respectively. The latter values overestimate the data of Agúndez et al. (2019) by factors of ∼2 and 3–5 in the case of HC_2NC and HNC_3, respectively.

IRC+10216. Our model failed at reproducing the observations with reasonable physical conditions. In fact, the H_2 densities (2.8×10^3 cm^{-3} and 8.0×10^4 cm^{-3} for HC_2NC and HNC_3, respectively) do not agree with the value of $(2.3–4.6) \times 10^4$ cm^{-3} derived using the mass loss rate of Guélin et al. (2018) at 14″ where Agúndez et al. (2017) observed the peak intensity of HC_3N. We used a temperature of 37 K as suggested by the finding of Guélin et al. (2018). We note that our model reproduces the observations with realistic gas densities only if the temperature is decreased down to ∼10 K. This failure may originate from the simplicity of our model which does not take the strong temperature and density gradients into account in IRC+10216. Moreover, in our model the excitation is exclusively due to the collision with H_2, whereas Agúndez et al. (2017) show that infrared pumping plays a huge role in the calculation of the HC_3N radial abundance distribution. Therefore, accurate modelling of the HC_2NC and HNC_3 abundances must be performed using more sophisticated radiative transfer codes.

3.3. The HC_2NC/HNC_3 abundance ratio in cold environments

The abundance ratios (r) were determined taking into account the dependence of the derived column densities (N_i, $i = \{1, 2\} \equiv \{HC_2NC,\ HNC_3\}$) on the H_2 volume density, that is $r(n) = N_1(n)/N_2(n)$. Since the χ^2 parameter behaves the same way for both isomers, this procedure helps to reduce the uncertainty. A good constrain of these data can lead to important clues regarding the chemistry underlying the formation and destruction processes of the isomers. In fact, despite being characterized by similar physical conditions, cold molecular clouds

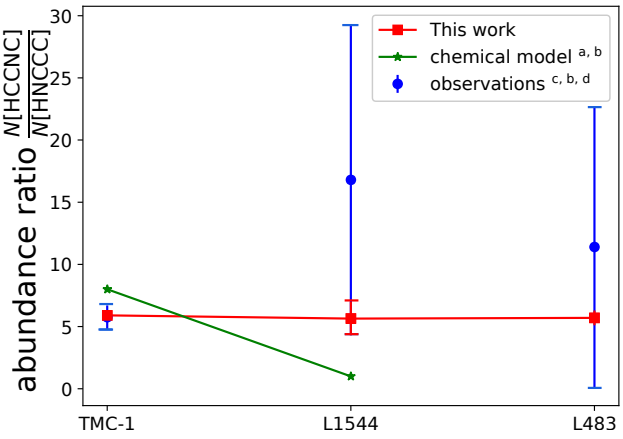

Fig. 4. Relative abundance of HC_2NC with respect to HNC_3 in cold environments. The subscripts ^{a,b,c} and ^{d} refer to Osamura et al. (1999), Vastel et al. (2018a), Cernicharo et al. (2020a), and Agúndez et al. (2019), respectively.

(TMC-1, L1544, and L483) present very different relative abundances for the isomers of HC_3N, according to the data available in the literature. Typically, when interpreting the observational spectra, the ratio obtained for L483 (Agúndez et al. 2019) is twice as great as the relative abundance reported for TMC-1 (Cernicharo et al. 2020a). For L1544 (Vastel et al. 2018a), there is nearly a factor of 7 between the lower and the upper limits of the interval of the abundance ratio.

Regarding chemical models, the abundance ratio computed by Osamura et al. (1999) for TMC-1 overestimated the observations of Cernicharo et al. (2020a) by nearly a factor of 1.5. For L1544, the chemical model of Vastel et al. (2018a) predicts nearly the same amounts of HC_2NC and HNC_3. These authors state that their model overestimates the abundance of HNC_3 by a factor of 5–10 relative to the observations.

In this work, we obtained very close abundance ratios for all of the molecular clouds studied (TMC-1, L1544, and L483); readers can refer to Table 2 for the exact values. For a better appreciation of the ratios obtained, we show a comparison of these abundance ratios with the previous estimates in Fig. 4. With respect to the observations, our model agrees with Cernicharo et al. (2020a), constrains the interval derived from Vastel et al. (2018a), and reduces the results of Agúndez et al. (2019) by a factor of 1.5–2.5. For the chemical models, our findings are in reasonable agreement with the data of Osamura et al. (1999), but they are incompatible with those of Vastel et al. (2018a) since their model predicts equal amounts for HC_2NC and HNC_3.

4. Conclusion

We performed non-LTE radiative transfer calculations to estimate the impact of the new rate coefficients on the excitation scheme of HC_2NC and HNC_3 and to model the abundance of the isomers in cold molecular clouds TMC-1, L1544, and L483 as well as the circumstellar envelope IRC+10216. We found that the use of the rate coefficients of HC_3N when investigating the excitation in the ISM of HC_2NC or HC_3N may lead to underestimation down to ∼15% or overestimation up to ∼40% for $10^4 \leq n(H_2)\ (cm^{-3}) \leq 5\times10^4$. The deviations depend on the emission line, the kinetic temperature, and the isomer.

Using a fixed temperature for each astrophysical environment, we derived (i) the gas density of the cold media which agrees fairly well with the results in the literature and (ii) the column density of the isomers. For the latter, we found significant differences with respect to the previous modelling performed for TMC-1, L1544, and L483. In contrast with previous determinations of the $N(HC_2NC)/N(HNC_3)$ abundance ratios, focused on an individual source each, which found a high dispersion of values, our simulation suggests similar ratios in cold media. This finding, supplemented by the fact that TMC-1, L1544, and L483 are characterized by similar physical conditions, let us believe that the same chemistry governs the formation and destruction paths of HC_3N, HC_2NC, and HNC_3 in these cold media. Due to the simplicity of our model which does not take the temperature and density gradients of IRC+10216 into account, we could not reproduce the observational spectra with reasonable gas densities. We expect that the problem discussed in this paper will encourage further modelling with more robust non-LTE radiative transfer tools and future studies to revisit the chemistry of HC_3N and its isomers in cold molecular clouds.

Acknowledgements. The authors acknowledge the Programme National "Physique et Chimie du Milieu Interstellaire" (PCMI) of Centre National de la Recherche Scientifique (CNRS)/Institut National des Sciences de l'Univers (INSU) with Institut de Chimie (INC)/Institut de Physique (INP) co-funded by Commissariat a l'Energie Atomique (CEA) and Centre National d'Etudes Spatiales (CNES). This project has received funding from the European Research Council (ERC) under the European Union's Horizon 2020 research and innovation programme (Grant agreement No. 811363). This work was granted access to the Occigen HPC resources of CINES under the allocation 2019 [A0070411036] made by GENCI. F.L. acknowledges the Institut Universitaire de France. The authors warmly acknowledge fruitful discussions with Marcelo Agúndez.

References

Adler, T. B., Knizia, G., & Werner, H.-J. 2007, J. Chem. Phys., 127, 221106
Agúndez, M., Cernicharo, J., Quintana-Lacaci, G., et al. 2017, A&A, 601, A4
Agúndez, M., Marcelino, N., Cernicharo, J., Roueff, E., & Tafalla, M. 2019, A&A, 625, A147
Bop, C. T., Batista-Romero, F. A., Faure, A., et al. 2019, ACS Earth Space Chem., 3, 1151
Bop, C. T., Lique, F., Faure, A., Quintas-Sánchez, E., & Dawes, R. 2021, MNRAS, 501, 1911
Botschwina, P., Horn, M., Seeger, S., & Flügge, J. 1992, Chem. Phys. Lett., 195, 427
Cernicharo, J., Marcelino, N., Agúndez, M., et al. 2020a, A&A, 642, A8
Cernicharo, J., Marcelino, N., Pardo, J., et al. 2020b, A&A, 641, A9
Cordiner, M., Buckle, J., Wirström, E., Olofsson, A., & Charnley, S. 2013, ApJ, 770, 48
Endres, C. P., Schlemmer, S., Schilke, P., Stutzki, J., & Müller, H. S. 2016, J. Mol. Spectr., 327, 95
Faure, A., Lique, F., & Wiesenfeld, L. 2016, MNRAS, 460, 2103
Gensheimer, P. 1997, ApJ, 479, L75
Gensheimer, P. D. 1998, in Dust and Molecules in Evolved Stars, eds. I. Cherchneff, & T. J. Millar (Dordrecht: Springer Netherlands), 199
Green, S. 1975, J. Chem. Phys., 62, 2271
Guélin, M., Patel, N., Bremer, M., et al. 2018, A&A, 610, A4
Hill, J. G., Mazumder, S., & Peterson, K. A. 2010, J. Chem. Phys., 132, 054108
Jiménez-Serra, I., Vasyunin, A. I., Caselli, P., et al. 2016, ApJ, 830, L6
Kawaguchi, K., Ohishi, M., Ishikawa, S.-I., & Kaifu, N. 1992a, ApJ, 386, L51
Kawaguchi, K., Takano, S., Ohishi, M., et al. 1992b, ApJ, 396, L49
Krüger, M., Dreizler, H., Preugschat, D., & Lentz, D. 1991, Angewandte Chem. Int. Ed. Engl., 30, 1644
Osamura, Y., Fukuzawa, K., Terzieva, R., & Herbst, E. 1999, ApJ, 519, 697
Pratap, P., Dickens, J., Snell, R. L., et al. 1997, ApJ, 486, 862
Quénard, D., Vastel, C., Ceccarelli, C., et al. 2017, MNRAS, 470, 3194
Van der Tak, F., Black, J. H., Schöier, F., Jansen, D., & van Dishoeck, E. F. 2007, A&A, 468, 627
Vastel, C., Ceccarelli, C., Lefloch, B., & Bachiller, R. 2014, ApJ, 795, L2
Vastel, C., Kawaguchi, K., Quénard, D., et al. 2018a, MNRAS, 474, L76
Vastel, C., Quénard, D., Le Gal, R., et al. 2018b, MNRAS, 478, 5514
Wernli, M., Wiesenfeld, L., Faure, A., & Valiron, P. 2007, A&A, 464, 1147

Appendix A: Optical depth of the HC_2NC and HNC_3 emission lines

In this section, we present the dependence of the optical depths (τ) of the HC_2NC and HNC_3 emission lines on the H_2 volume density for selected temperatures. We used column density values of $10^{12}\,cm^{-2}$ and $10^{11}\,cm^{-2}$, similar to those derived in our fit, for HC_2NC and HNC_3, respectively. Figs. A.1 and A.2 show very low opacities, suggesting that the lines are optically thin. Since τ is proportional to the column density, using higher column densities does not change the optically thin regime.

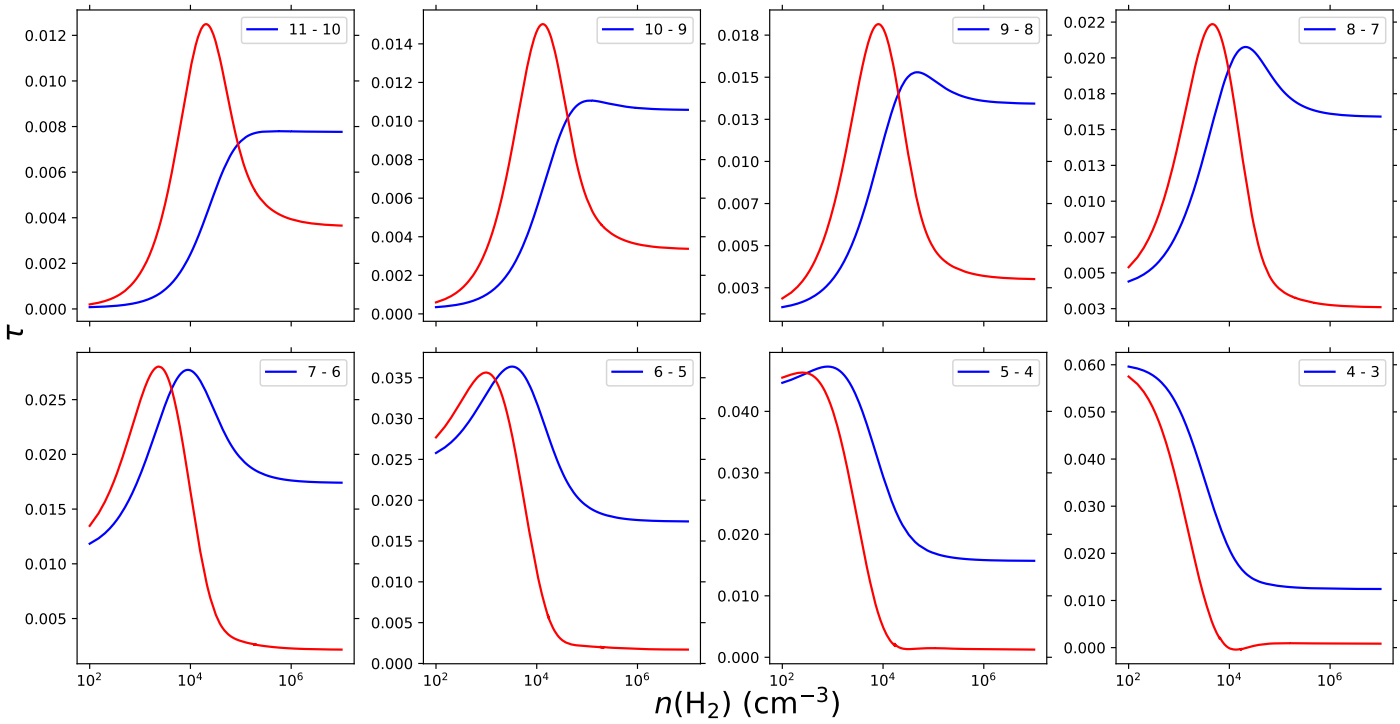

Fig. A.1. Dependence of the optical depth for the HC_2NC observed emission lines on the gas density for selected temperatures. The blue and red lines stand for temperatures of 10 K and 40 K, respectively. The calculations were performed using a column density of 10^{12} cm^{-2}.

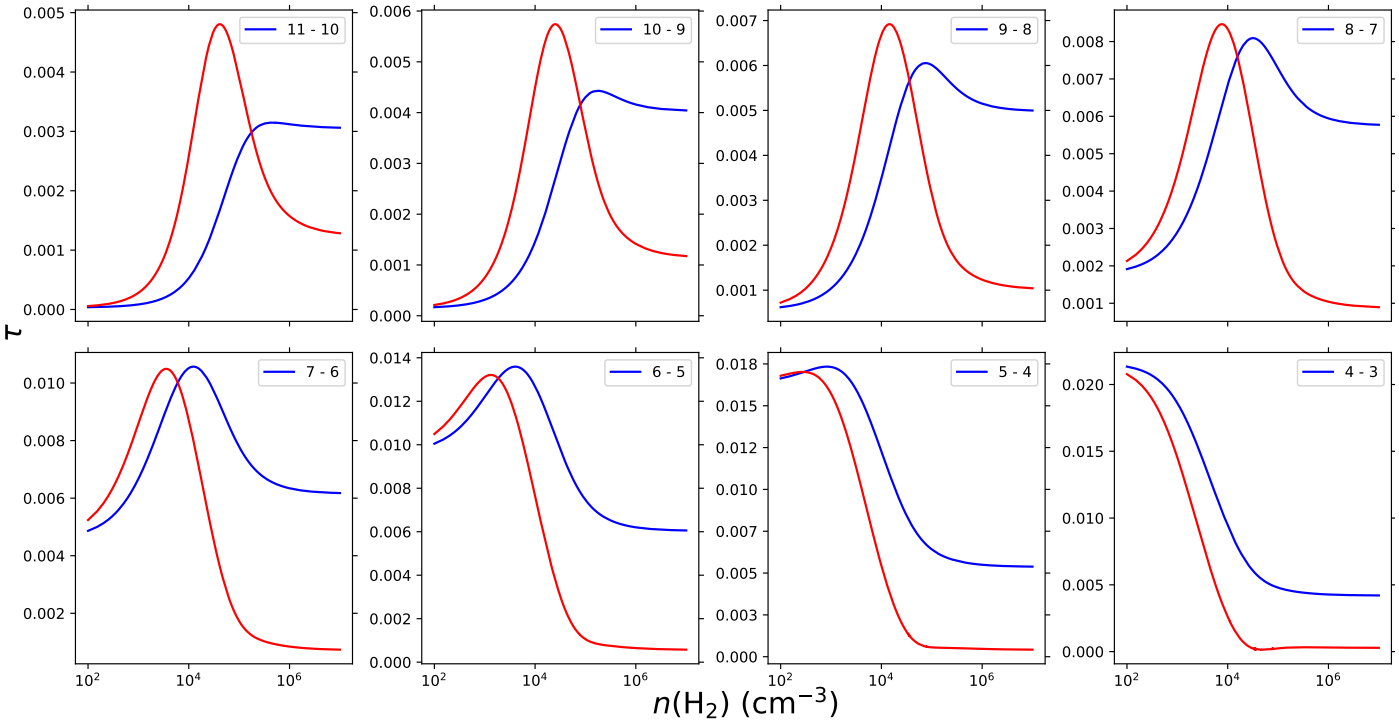

Fig. A.2. Same as Fig. A.1, but for HNC_3 using a column density of 10^{11} cm^{-2}.